Published in final edited form as:
NMR Biomed. 2013 September ; 26(9): 1125–1134. doi:10.1002/nbm.2926.

Magnetic Resonance Imaging Confirms Loss of Blood- Brain Barrier Integrity in a Mouse Model of Disseminated Candidiasis

Dhammika H. M. L. P. Navarathna[1], **Jeeva Munasinghe**[2], **Martin J. Lizak**[2], **Debasis Nayak**[2], **Dorian B. McGavern**[2], and **David D. Roberts**[1,*]

[1]Laboratory of Pathology, Center for Cancer Research, National Cancer Institute, National Institutes of Health, Bethesda, MD 20892

[2]National Institute of Neurological Disorders and Stroke, National Institutes of Health, Bethesda, MD 20892

Abstract

Disseminated candidiasis primarily targets the kidneys and brain in mice and humans. Damage to these critical organs leads to the high mortality associated with such infections, and invasion across the blood- brain barrier can result in fungal meningoencephalitis. *Candida albicans* can penetrate a brain endothelial cell barrier *in vitro* through transcellular migration, but this mechanism has not been confirmed *in vivo*. MRI imaging using the extracellular vascular contrast agent Gd-DTPA demonstrated that integrity of the blood- brain barrier is lost during *C. albicans* invasion. Intravital two-photon laser scanning microscopy was used to provide the first real time demonstration of *C. albicans* colonizing the living brain, where both yeast and filamentous forms of the pathogen were found. Furthermore, we adapted a previously described method utilizing MRI to monitor inflammatory cell recruitment into infected tissues in mice. Macrophages and other phagocytes were visualized in kidney and brain by administering ultra-small iron oxide particles. In addition to obtaining new insights into the passage of *C. albicans* across brain microvasculature, these imaging methods provide useful tools to further study the pathogenesis of *C. albicans* infections, define the roles of *Candida* virulence genes in kidney versus brain infection, and assess new therapeutic measures for drug development.

Keywords

Candida albicans; murine disseminated candidiasis; blood- brain barrier; magnetic resonance imaging; extracellular vascular contrast agent Gd-DTPA; ultra small iron oxide particles; intravital two photon microscopy

Introduction

Candida albicans is a commensal in the human gastrointestinal tract and the most common fungal pathogen of humans. It is the fourth leading cause of nosocomial infections in the United States. Disseminated candidiasis is often fatal in immunocompromised individuals, although superficial infections such as oral thrush and vaginal yeast infections also affect immunocompetent individuals (1). Several aspects of human disseminated candidiasis can be effectively modeled in mice, which have contributed much to our present understanding of the pathogenesis to *C. albicans* infections and host immune responses to infection (2). Kidney and brain are the primary target organs of this organism during infection. Within the

*Correspondence: NIH, Building 10 Room 2A33, 10 Center Drive, Bethesda, MD 20892-1500, Tel: 301-594-5256, Fax: 301-402-0043, droberts@helix.nih.gov.

kidney, massive fungal invasion and growth can occur, resulting in inflammatory reactions that lead to tissue necrosis (3).

C. albicans also invades the brain during acute infections and causes meningoencephalitis (4). Fifty percent of patients with disseminated candidiasis have CNS fungal invasion, which is associated with a mortality rate reaching 90% (5–6). *Candida* is the second most common contaminant cause of brain abscess formation due to hematopoietic stem cell transplantation (7). *C. albicans* has also been reported to cause meningoencephalitis without systemic infection in healthy individuals (8). Brain infection results in micro-abscesses mostly in the junctional area between white matter and gray matter. Basal ganglia and other cerebral regions are frequently involved (5). These micro-abscesses are surrounded by inflammatory cells. *Candida* hyphae can spread without inflammatory reactions in immunocompromised individuals (9).

The mode by which *C. albicans* enters brain tissues from circulation is not entirely understood. *In vitro* studies using cultured endothelial cells demonstrated that *C. albicans* can penetrate an endothelial cell barrier by trans-cellular migration (10). A more recent study showed that invasion of brain endothelial cells by *C. albicans* is mediated by the fungal invasins Als3 and Ssa1 (11). Als3 binds to the heat shock protein gp96 on brain endothelium, which promotes endocytic uptake. Another study using neonatal rodents suggested that *C. albicans* is engulfed in an ICAM-1-expressing vesiculo-vacuolar structure before migrating transcellularly across the blood-brain barrier (BBB) (12). Nevertheless, meningoencephalitis in this rat model could only be reproducibly demonstrated following intracerebral inoculation. Studies in other species have shown that the BBB becomes leaky during pathogenesis (13). However, to our knowledge the effects of *Candida* infections on vascular integrity of the brain and kidney have not been visualized *in vivo*.

MRI of ultra-small particles of iron oxide (USPIO) contrast agents has been used to study phagocyte recruitment in an arthritis model (14–16), for detecting *Pseudomonas aeruginosa* in a burn model (17), osteomyelitis (18–21), toxoplasmosis in brain (22), and *Staphylococcus aureus* in soft tissue (23–26). MRI with USPIO contrast agents have been used in kidneys for detection of allograft rejection (27–30) and inflammation following ischemia (31). Cellular infiltration associated with inflammation was visualized by MRI 24 h following intravenous injection of USPIO (32–33).

Intravital imaging of living brain and its vasculature during infection has become an important experimental tool for understanding the dynamics of CNS infectious disease processes in real time (34). Yang et al. recently developed a detailed protocol for imaging cortical structures at high optical resolution through a thinned-skull cranial window in live mice using two-photon laser scanning microscopy (TPLSM) (35). The experimental procedure can be performed multiple times, which allows longitudinal imaging of the meninges and cortex over specific time intervals. Importantly, when compared to craniotomies, the thinned skull preparation is far less injurious and permits study of brain structure and function in the live animals in states of health and disease.

Here, we present an infection model using a GFP-expressing virulent *Candida* strain (36) to directly visualize for the first time *Candida* cells colonizing the brain. Further, we use MRI to noninvasively examine BBB integrity and to monitor inflammatory changes in infected kidneys and brains by imaging macrophages and other phagocytes containing USPIO during disseminated candidiasis in mice. We provide data showing that the BBB is breached following *Candida* infection and document a strategy to non-invasively monitor inflammation severity in the brain and kidney by MRI.

Experimental

Strains and growth conditions

C. albicans wild type (WT) strain SC5314 was used for mouse model studies. For challenge of mice, *C. albicans* cells were grown overnight in 50 ml of Yeast Peptone Dextrose (YPD) medium at 30°C with aeration as previously described (37). Cells were harvested by centrifugation at 5000 rpm for 10 min, washed twice with 50 ml of sterile non-pyrogenic normal saline (Quality Biological Inc. Gaithersburg, MD), and resuspended in 10 ml of saline before quantifying cell numbers using a Petroff-Hausser counting chamber. The cell suspensions were adjusted to the final concentration for parenteral administration using non-pyrogenic sterile saline. For intravital two photon microcopy studies, we used a GFP-expressing recombinant *C. albicans* strain (36).

Mouse infection with *C. albicans*

Eight to twelve week-old (18–20 g) BALB/c mice were used for all animal experiments. Mice were randomly allocated to groups of 5–6 animals and housed and cared with ad libitum access to filtered water and standard mouse chow. Handling and care of animals was conducted in compliance with the guidelines established by the Animal Care and Use Committee of the National Cancer Institute. Each group of mice was inoculated intravenously in the lateral caudal tail vein using a 30 gauge needle with a volume of 0.1 ml containing 5×10^5 *C. albicans* cells (3,37). This level of infection induces subacute candidiasis in mice with meningoencephalitis and kidney inflammation at 1, 3 and 5 days post inoculation (PI). These time points were selected for MRI experiments unless otherwise indicated. We examined 5 mice per group at days 0, 1, 3 and 5 post-infection (PI) to monitor level of BBB breach and inflammatory changes. As the disease progress we noticed that sick mice lost weight and slightly dehydrated. Clinical signs of illness in each mouse were evaluated three times daily, and mice that displayed severe signs were euthanized immediately by CO_2 inhalation and processed for complete necropsy and collection of tissues for histopathological examination.

Magnetic Resonance Imaging

MRI experiments were performed on 7-T, horizontal Bruker (Bruker Biospin Inc. Billerica, MA) Avance (brain) and Bruker Pharmascan (Kidney) scanners. At least 5–6 mice were used for each experimental treatment. Mice at 1, 3 and 5 days PI were anesthetized with 1.5% isofluorane and positioned in a stereotaxic holder. The body core temperature was maintained at 37° C using circulating water and monitored by means of a rectal temperature probe. A line through the tail vein was placed for contrast agent infusion. Magnevist® is an FDA approved Gadolinium-DTPA contrast agent for MR imaging. It is supplied as a 0.5 mmol/ml solution. The recommended dose for mice is 0.05–0.5 mmol/kg (0.1–1.0 ml/kg) body weight IV, and we administered at 0.25 mmol/kg (0.5 ml/kg). A pressure transducer was positioned to monitor respiration. During MRI of kidney this signal was synchronized with data acquisition to minimize motion-related image artifacts.

BBB integrity study

The mouse's head was centered in a 72/25 mm transmit/receive coil ensemble, and three mutually perpendicular scout images were acquired. T_1-weighted axial images (Repetition Time [TR]/Echo Time [TE] = 200/5.9 ms, slice thickness = 1, number of averages = 8, Matrix = 256^2, FOV= 1.92 cm) encompassing the whole brain were acquired using a Gradient Echo (GE) sequence, before and 5 minutes, after administration of a bolus of Gd-DTPA (0.2 cm^3/kg body weight). In order to assess the relative breaching of the BBB, multiple sites in the brain was evaluated with regions of interest (ROI) placed in the cortices

of both hemispheres (Fig. 1A). Dynamic contrast imaging and brain average spin-spin relaxation times (T_2) and apparent diffusion coefficients (ADC) were analyzed using a separate set of 6 mice per group at day 3 PI using an Echo Planar Imaging (EPI) gradient echo sequence (SW= 350 KHz, TE = 22 ms, temporal resolution = 2 s, Matrix size=128^2, FOV=1.92 cm) after a bolus of Gd-DTPA. Nine contiguous T_2 (TE = 12 ms, 16 echos, Matrix size=128^2, FOV=1.92 cm) and diffusion (TE= 15 ms, Δ = 20 ms, b values = 0, 1000 mm/s - along read gradient axes, Matrix size=128^2, FOV=1.92 cm) weighted axial images, originating 2 mm posterior to the olfactory bulb, were acquired. Scanned animals were then perfused under anesthesia to remove blood from the circulatory system and brain histology studied. Unless otherwise mentioned, all the MRI experimental procedures were reproduced at day 0, 1, 3 and 5 PI representing at least 5 mice per group.

Kidney and Brain inflammation study

Macrophage and other phagocyte infiltration of the kidneys and brains was observed using USPIO (Molday ION™ BIOPaL, MA). Each mouse was given 0.015 ml of Molday ION dissolved in 0.1 ml of sterile saline 24 hrs. before the scan. T_2^*-weighted images of the kidneys were acquired using a FLASH sequence. using 6 mice per group at 3 days post inoculation and 24 hours following administration of the USPIO contrast agent were used for preliminary qualitative experiments compared with the control mice. Thereafter, 5 mice representing each experimental replicate at 1, 3 and 5 days PI were used for quantitative analysis at each time point to compare the progression of kidney and brain pathology. After anesthesia was induced, each mouse was positioned on a holder with its face in an anesthesia mask and its legs extended to the front and back. The mouse was centered in a 35 mm linear bird cage coil, and twelve 1 mm slices were acquired through the length of the body using a GE sequence (FOV = 5.0×3.2 cm, TE=10 ms, 30 degree flip angle, 256×256 matrix, NA=4). In order to reduce motion artifacts, acquisition was synchronized with the breathing sensor. This yielded an effective TR of approximately 1500 ms. A separate cohort of mice were scanned on a second 7T Bruker scanner. The set up was identical to the BBB Gd study where the mouse's head was centered in a 72/25 mm transmit/receive coil ensemble, and three mutually perpendicular scout images were acquired. T_1-weighted axial images (Repetition Time [TR]/Echo Time [TE] = 200/5.9 ms, slice thickness = 1, number of averages = 8, Matrix = 256^2, FOV= 1.92 cm) encompassing the whole brain were acquired using a Gradient Echo (GE) sequence.

Data Analysis

T_2, apparent diffusion coefficients (ADC), post Gd signal variation (expressed as relative contrast − [{Pre Gd− post Gd}/pre Gd] × 100) for series of selected anatomical areas (10 ROIs per region in cortex and 2 ROIs per region in hippocampus, with 10 pixel area of 5.625×10^{-4} cm^2), and temporal variation of signal in dynamic contrast images (Fig. 1E-X and 1-E-Y, 1 ROIs per region in cortex and hippocampus, with 10 pixel area of 5.625×10^{-4} cm^2) were calculated using MATLAB (Mathworks Inc., Natick, MA) routines. Statistics of signal intensities in time points and flow cytometry data were analyzed using GraphPad Prism software.

Necropsy and Histopathology

Immediately after euthanasia, macroscopic changes were recorded, and the brain, heart, lungs, liver, spleen, and right kidneys were immersed in buffered 10% formalin, processed for paraffin embedding, sectioned at 5 μm, and stained with H&E. Grocott's modification of Gomori's methenamine-silver (GMS) stain was used for detection of fungi in situ (38).

Microscopy

Histopathology images from sections of formalin-fixed and paraffin-embedded tissues stained with Gomori's methenamine-silver or hematoxylin and eosin were obtained using ScanScope XT digital scanner (aperio). Images were processed using Aperio ImageScope v11.1.2.760 (aperio).

Mononuclear cell isolation

To obtain cell suspensions for flow cytometric analysis and sorting, brains were harvested from mice after an intracardiac perfusion with 20 ml of 0.9% saline solution to remove contaminating blood lymphocytes. The brain was incubated with 1 ml of collagenase D (1 mg/ml, Roche) at 37°C for 30 min. Single-cell suspensions were prepared by mechanical disruption through a 100 μm filter. Brain-infiltrating leukocytes were isolated and counted as described previously (39). Five control mice and 5 *C. albicans* infected mice at day 3 PI were compared.

Flow cytometry

Leukocytes harvested from the brain were blocked with 3.3 μg/ml anti–mouse CD16/CD32 (Fc Block; BD) in PBS containing 1% FBS and 0.1% sodium azide for 10 min on ice. Cells were surface stained with a combination of the following conjugated antibodies: anti-CD45.2 FITC (BD; Clone 104), Gr-1 PE (eBioscience; Clone RB6-8C5), Thy1.2 Alexa 700 (Biolegend; Clone 30-H12), CD11b PE/Cy7 (M1/70; eBioscience), CD11c Pacific Blue (Biolegend; Clone N418), and Ly6C PerCP Cy5.5 (BD; Clone AL-21) for 20 min on ice. Cells were acquired using a digital flow cytometer (Digital LSR II; BD), and flow cytometric data were analyzed with FlowJo software (Tree Star, Inc).

Intravital two-photon microscopy

Intravital two-photon laser scanning microscopy was conducted as previously reported (40). Briefly, mice were anaesthetized and maintained on a metal plate at 37°C. Prior to anaesthetizing the mice, 100 μl of normal saline containing 5 μl of 655 nm emission quantum dots (0.2 μm; Invitrogen) was administered intravenously to visualize the vasculature. A surgical window in the intact skull was made as previously described (35,41). Briefly, a 0.5 to 1.0 mm-diameter area of the skull was thinned gently to a thickness of ~40–50 μm using a sterile drill and further thinned to ~20 μm manually using a microblade. Prior to imaging, some mice were injected intravenously with 10^6 GFP^+ *C. albicans.* Imaging data shown in Fig. 4 and supplemental Movie 1 were collected using a Leica SP5 two-photon imaging system equipped with an 8,000-Hz resonant scanner, a 20× (1.0 NA) dipping objective, and a Mai Tai DeepSee Laser (Spectra-Physics) tuned to 920 nm. Fluorescence emission was separated by high-efficiency custom dichroic mirrors (Semrock) and collected with a NDD4 external detector (Leica). Image stacks of 1 μm were acquired at 2 min intervals up to a depth of 100 μm below the skull bone. Imaging through the thinned skull region was conducted for two hours in uninfected and day 3 infected mice. All 4D data were processed using Imaris 7.0 software (Bitplane) and Adobe Premiere CS4.

Results

Gd-DTPA is an intravascular contrast agent in the brain that does not cross the intact BBB. Thus, minimal contrast signal was seen in normal brains (Fig. 1A). However, post-Gd images of infected brains revealed increased image contrast at 1, 3 and 5 days PI (Fig. 1B–D), indicating Gd-DTPA leakage.

Dynamic contrast studies for selected cortical and hippocampal ROIs (2 ROIs per region with pixel resolution of 0.0075 cm and 10 pixel area of 5.625×10^{-4} cm^2, Fig. 1E) showed

distinct first pass recovery of Gd-DTPA signal in normal mice (Fig. 1F), consistent with studies on brains with intact BBB. In contrast, many ROIs in the infected mouse brain exhibited a curve associated with vascular leakage/T_1 relaxation effects (Fig. 1G). The fact that recovery curves in all ROIs in the infected mice did not show leakage (data not shown) indicates that *Candida* infiltration results in focal breaching of the BBB. Loss of BBB integrity was quantified by Gd-DTPA infusion into selected regions of interest (10 ROIs per region with 10 pixel area of 5.625×10^{-4} cm^2) in the brain frontal cortex of *C. albicans*-infected and uninfected mice (Fig. 1H). Arbitrary values of signal variation in all six cortical ROIs averaged over 10 contiguous slices show extensive disruption of BBB function in infected brains (Fig. 1I). Similar trends were also observed in other regions such as hippocampal and caudate areas (2 ROI per region with 10 pixel area of 5.625×10^{-4} cm^2 in each, data not shown).

The post-Gd-DTPA contrast images also showed variable localization of hyper-intense signals in the longitudinal study at 1, 3 and 5 day PI compared with the control uninfected mice (Fig 2A vs 2B,C and D), indicating that the sites where BBB integrity is lost vary among the studied mice. Notably, loss of BBB integrity was closely associated with *C. albicans* infiltration detected in the corresponding fungal-specific GMS stained slides (Fig. 2F–H arrows and 2J-Lhigher magnification showing fungal colonization of the demarcated area in the respective images). A high degree of alignment was observed between *C. albicans* colonization and areas of higher Gd image contrast (Fig. 2). MRI of uninfected brains (Fig 2A) and corresponding GMS stained sections (Fig. 2E and I) demonstrate that uninfected mice do not leak Gd-DTPA through the BBB.

Average T_2 values of infected cortex were significantly lower than in control mice (Fig. 3A). However, T_2 variations in other anatomical structures such as hippocampus were not significant (46.7 ± 3.8 ms for infected versus 49.3 ± 3.7 for normal). In contrast, BBB disruption and infection was not sufficient to significantly alter apparent diffusion coefficient (ADC) values (Fig. 3B), at least in the measured direction. This study was not designed to understand detailed brain T_2 and ADC variations but concentrated on quantifying longitudinal changes during *C. albicans* infection.

We extended the post-Gd-DTPA contrast imaging to study longitudinal effects of candidiasis in breaching the BBB. As early as day 1 PI, mice infected with *C. albicans* showed significantly hyper-intense signals compared with the non-infected control mice ($p<0.05$, Fig. 3C). However, the maximal signal intensity compared with control mice occurred on days 3 and 5 PI ($p<0.001$).

C. albicans colonizes the meninges and brain parenchyma

To provide direct *in vivo* evidence that *C. albicans* actively colonizes the brain when the BBB is disrupted, we visualized GFP-tagged *Candida* by intravital TPLSM at 30 min to day 3 post-infection. Virulence of the GFP^+ strain reported by Igyarto et al., (36) was confirmed by conducting a survival study following injection of 10^6 cells per mouse. All five of the infected mice died within seven days, and gross pathology/histopathology were similar to that observed in mice infected with other virulent WT strains (data not shown). Although we observed sporadic entry of fluorescent *Candida* yeast cells into the brain parenchyma as early as a 30 min time point, these events were too infrequent within the accessible field of imaging to acquire a statistically significant sample(data not shown). When compared to uninfected controls, we observed both yeast and filamentous forms of GFP^+ *C. albicans* by TPLSM in the living brains of mice at day 3 post-infection (Fig. 4, supplemental Movie 1). *Candida* was visible in meninges and underlying brain parenchyma. In addition, clear evidence of filament elongation was observed over the two hour observation period. There

were also examples of highly motile GFP^+ signal, suggesting that some of the yeast were migrating inside of phagocytes.

Histopathology of *Candida* infected brains

Candida invasion of the brain primarily involved cerebrum and subcortical regions. Numerous *Candida* filaments were in areas of malacia, especially in gray matter. *C. albicans* was observed in the choroid plexus of the lateral ventricles. Fungi were accompanied by inflammation and sometimes hemorrhages (data not shown). We also observed *C. albicans* and infiltrating mononuclear cells in the cerebral leptomeninges. Inflammatory reactions were pyogranulomatous consisting of a mixture of neutrophils and macrophages. We did not observe *Candida* or inflammation in the cerebellum and medulla.

Assessment of phagocyte infiltration by MRI

Macrophage and other phagocyte infiltration were confirmed by MRI analysis of infected kidneys and brains. T_2^* weighted imaging studies were performed in infected mice administered *i.v.* USPIO to label phagocytic cells. Organs from each mouse were then stained with GMS to visualize the *Candida* and H&E to visualize host inflammatory cells. The top panels of Fig. 5 shows representative MRI sections through the kidneys of *Candida* infected kidneys without USPIO (A), non-infected kidneys without USPIO (B), non-infected kidneys with USPIO (C) and infected kidneys with USPIO (D). The respective lower panels show GMS and H&E stained sections of the same kidneys harvested after imaging. *Candida* infected kidneys without USPIO (A) and non-infected with or without USPIO (B,C) showed no differences in contrast, demonstrating specificity of the USPIO contrast signal for infected kidneys.

Kidneys of infected mice had widespread inflammatory cell infiltration of the kidneys visible by MRI as signal dropouts in affected areas (Fig. 5D top panel). Fungal-specific GMS staining confirmed the presence of fungi, and H&E staining of sections from the same kidneys confirmed heavy colonization by *C. albicans* and massive inflammatory reactions containing neutrophils, monocytes, and macrophages.

Next, we monitored the level of kidney and brain infection in a longitudinal study. We compared non-infected mice administered USPIO with *Candida*-infected mice at day 1, 3 and 5 PI (Fig. 6A). We demarcated three kidney regions: medullar, corticomedullar, and cortex to study T_2^* signal perturbation due to adsorbed USPIO. We found that signal intensities representing each area were significantly lower than in control mice ($p<0.001$, Fig. 6A right panels). In the same manner we examined frontal and dorsal parts of the cerebrum (10 ROIs per region with 10 pixel area of 5.625×10^{-4} cm^2 per slice) for perturbation of signal due to USPIO-laden phagocytes (Fig. 6B). At all time points post-infection, both regions of brains showed significantly lower signal intensity ($p<0.001$). To confirm the presence of phagocytes/leukocytes in the brain during candidiasis, we conducted a parallel flow cytometric study to monitor brain-infiltrating leukocytes. We found that both the percentage and absolute number of neutrophils, ratio of monocytes to macrophages, and dendritic cells were significantly higher in *Candida*-infected brains compared with the non-infected controls (Fig. 6C). This validates our interpretation of the signal perturbation in the brain by USPIO during *Candida* infection.

Discussion

Incomplete understanding of the trafficking of CNS fungal infections has been a major obstacle for managing *Candida* meningoencephalitis. The structural and functional BBB protects the CNS, and an infecting microbe must pass through this BBB to invade the CNS.

The BBB is formed by brain microvascular endothelial cells, the underlying basement membrane, as well as associated astrocytes and pericytes. Brain microvascular endothelial cells have uniquely tight junctions and exhibit very limited pinocytosis (42). Microbes have been shown to cross the BBB by three mechanisms to reach the CNS: transcellular, pericellular (microbial penetration between cells with or without disrupting tight junctions), and Trojan horse routes (transmigration within infected phagocytes). Transcellular breaching of the BBB accounts for most meningoencephalitis caused by bacterial pathogens such as *E. coli*, *S. agalactiae* and *N. meningitidis*. This process shows no evidence of tight junction disruption (25). *In vitro* studies suggested that the fungal pathogen *Cryptococcus neoformans* uses a transcellular route to cross the BBB (43), and similar *in vitro* studies have inferred that this is the mechanism used by C*. albicans* to enter the CNS and cause meningoencephalitis (10). In fact, recent data support a model by which C. albicans accesses brain endothelium by binding to the heat shock protein, gp96 (11). However, it remains to be determined if this is the preferred route of CNS entry used *in vivo* by *C. albicans.*

To advance our understanding of *C. albicans* pathogenesis *in vivo,* we combined MRI imaging, intravital TPLSM, and histopathology to clarify the genesis of *C. albicans* meningoencephalitis. MRI enabled the evaluation of BBB integrity during *Candida* infiltration using the contrast agent Gd DTPA and quantitative T_2 diffusion imaging. We attempted to visualize actual entry events by a two photon microscopic study. We found that Candida exits the brain vasculature as early as 30 min post inoculation and undergoes dynamic filamentation by 3 day PI. This revealed the interesting observation that most yeast cells outside the vasculature show dynamic movement that can be explained by their engulfment by motile phagocytic cells. In contrast, hyphal cells show only slow invasion based on hyphal extension. Although we consistently observed sporadic entry of fluorescent *Candida* yeast cells into the brain parenchyma as early as a 30 min time point, these events were too infrequent within the accessible field of imaging to acquire a statistically significant sample. We did not observe Gd-leakage as early as 30 min. Therefore, our methods cannot distinguish pericellular and transcellular crossing of the BBB, but we can state that entry initially occurs without gross disruption of the BBB.

It is also conceivable that BBB breakdown is caused by leukocyte infiltration. This could then promote further colonization of the brain by *Candida*. Regardless of the exact mode of entry, our intravital imaging data at day 3 post-infection revealed significant colonization and filament elongation by *C. albicans* in the meninges and parenchyma, which coincided temporally with BBB breakdown by MRI. The scattered distribution of *Candida* in the cerebrum and cortex seen on histopathology is also consistent with the MRI results. A similar distribution of brain lesions has been reported in cerebrum and cortex of humans infected with *C. albicans* (44). Another histological study of *Candida* infected human brains reported frequent lesions in the corticomedullary junction (5).

Our flow cytometry, histopathology, and MRI findings indicate that the brain becomes heavily inflamed at sites of *C. albicans* invasion, which supports other studies that have focused on CNS inflammation following *Candida* infection (5–6,8). The leaky BBB associated with *C. albicans* invasion may provide a route for inflammatory cells to enter the CNS. Conversely, production of reactive oxygen species and other factors by circulating monocytes and neutrophils that encounter *C. albicans* in the brain vasculature may enhance disruption of BBB integrity (45–46). Our studies cannot distinguish between these two possibilities.

Given that identical numbers of cells were administered, the heterogeneous invasion of *Candida* into the brains of different mice suggests that local responses and factors produced by the pathogen trigger breakdown of the BBB. Our intravital two photon microscopic study

and the MRI data clearly show that once *Candida* enters the brain it significantly alters the local microenvironment. The T_2 values provide evidence of a disrupted cortical layer. The high density of micro-abscesses surrounding the *Candida* cells upon infiltration into the brain (Fig. 2) likely plays a role in altering T_2 values compared with the non-infected brains. Extensive invasion of the pathogen may induce changes in the cortical architecture, which we expected would reduce the measured ADC due to increase in cellular structures within the microenviroment. However, vacuoles filled with a dilute solution that occupy a significant volume of the fungal cells may outweigh the changes in local neuroachitecture, rendering measured ADC non-significant in comparison to the uninfected brains. Furthermore, the shorter T_2 value of the infected tissue may bias the ADC measurement towards the healthy tissue value.

Kidneys are the other major organ of interest in disseminated candidiasis because liver, spleen, and heart do not show persistent colonization of *Candida* (47). We examined inflammatory reactions in kidneys and brains by imaging USPIO-laden phagocytes. Recruitment of neutrophils, macrophages and some lymphocytes to the site of colonization is a major component of antifungal immunity. However, the recruited phagocytes cannot control a disseminated *Candida* infection because yeast cells engulfed by macrophages and other phagocytes escape by undergoing germ tube differentiation. The damaged macrophages in turn release reactive oxygen species, which are harmful to host tissues (48). Therefore, limiting this innate inflammatory response to produce a balanced immune response is important to control pathogenesis. Based on the key role played by macrophages (49), we employed MRI imaging to follow phagocyte recruitment and dynamics in infected kidneys and brain. Systemically administered USPIO is phagocytosed by monocytic cells and macrophages (50) and eventually cleared by the liver reticuloendothelial system (51). USPIO contrast agents shorten MRI T_1, T_2 and T_2* relaxation times, resulting in detectable signal changes during imaging. Compared with the Gd-DTPA, iron oxide contrast is more sensitive, and single USPIO laden cells have been visualized by MRI (52). This technique has been widely utilized to image inflammatory responses in the CNS (53–54). Our USPIO studies in *Candida* infected mice revealed phagocytic infiltration of kidney, which was evidenced by widespread signal perturbation when compared to the control groups (Fig. 5). Furthermore, the signal perturbation could be monitored longitudinally in infected kidney and brain (Fig. 6), and our flow cytometric analyses confirmed the presence of myelomonocytic cells in the brains of infected mice. Our initial studies did not show abnormal ADC values in the brain infection. When we examined histopathology, irrespective of fungal colonization of the cerebral regions of the brain, we did not see micro abscesses with concentrated inflammatory cells. Even though we observed a significant increase of inflammatory phagocytes (Fig. 6C), they were heterogeneously spread throughout the cerebrum. This could be the reason that we did not see abnormal ADC values. This tool could be utilized for future studies to quantify organ colonization by *C. albicans* mutants with disrupted virulence genes, to quantify colonization by *C. albicans* in transgenic mice lacking genes that control various components of host antifungal immunity, and to study how antifungal drugs affect the distribution and persistence of *C. albicans* in the CNS and kidney.

In summary, our studies demonstrate that the BBB is focally damaged during disseminated candidiasis in mice. We also show by two-photon microscopy and histology that *C. albicans* productively colonizes to the brain parenchyma and meninges during the phase of active BBB disruption. Based on our studies, MRI could provide a valuable diagnostic tool for immunocompromised patients exhibiting CNS-associated clinical signs. Use of USPIO to noninvasively track phagocyte infiltration into kidneys and brain could similarly advance our understanding of inflammation associated with colonization of these tissues.

Movie 1 | *C. albicans* colonization of the brain during induction of fungal meningoencephalitis. A 4D time lapse movie captured by TPLSM through a thinned skull shows colonization of the meninges and superficial brain parenchyma by GFP^+ *C. albicans* (green). The representative mouse was infected intravenously 3 days earlier with 5×10^5 yeast cells, and intravital imaging was performed when the mouse presented with clinical signs such as ruffled hair, sunken eyes and arched back posture. Filamentous green thread-like structures represent GFP^+ *C. albicans* hyphae or pseudohyphae colonizing the brain parenchyma (white arrows). These filaments can be seen growing over time. Note that most of the nonfilamentous yeast cells are highly dynamic throughout the imaging period, suggesting their engulfment by motile phagocytic cells. Quantum dots were used to visualize the brain vasculature (red).

Supplementary Material

Refer to Web version on PubMed Central for supplementary material.

Acknowledgments

This work was supported by the Intramural Research Program of the NIH, National Cancer Institute, Center for Cancer Research (DDR, Z01 SC 009173) and National Institute of Neurological Disorders and Stroke (MJL, DBM).

We thank Dr. Brenda Klaunberg, Ms. Vivian Diaz, Ms. Danielle Donahue and Mr. Daryl Despres for kind support and help in the mouse imaging facility of National Institute of Neurological Disorders and Stroke.

Abbreviations

BBB	blood- brain barrier
PBMC	peripheral blood monocyte
Gd-DTPA	gadolinium diethylenetriaminepentaacetic acid
USPIO	ultra-small particles of iron oxide
GE	gradient echo
EPI	echo planar imaging
YPD	yeast peptone dextrose
GMS	Gomori's methenamine-silver

References

1. Kullberg, BJ.; Filler, SG. Candidemia. In: Calderone, RA., editor. Candida and Candidiasis. Washington, DC: ASM Press; 2002. p. 327-340.
2. Ashman RB. Protective and pathologic immune responses against Candida albicans infection. Front Biosci. 2008; 13:3334–3351.10.2741/2929 [PubMed: 18508436]
3. Navarathna DH, Hornby JM, Krishnan N, Parkhurst A, Duhamel GE, Nickerson KW. Effect of farnesol on a mouse model of systemic candidiasis, determined by use of a DPP3 knockout mutant of Candida albicans. Infect Immun. 2007; 75:1609–1618.10.1128/IAI.01182-06 [PubMed: 17283095]
4. Witek-Janusek L, Shareef MJ, Mathews HL. Reduced lymphocyte-mediated antifungal capacity in high-risk infants. J Infect Dis. 2002; 186:129–133.10.1086/341293 [PubMed: 12089675]
5. Pendlebury WW, Perl DP, Munoz DG. Multiple microabscesses in the central nervous system: a clinicopathologic study. J Neuropathol Exp Neurol. 1989; 48:290–300. [PubMed: 2649643]

6. Sanchez-Portocarrero J, Perez-Cecilia E, Corral O, Romero-Vivas J, Picazo JJ. The central nervous system and infection by Candida species. Diagn Microbiol Infect Dis. 2000; 37:169–179.10.1016/S0732-8893(00)00140-1 [PubMed: 10904190]
7. Hagensee ME, Bauwens JE, Kjos B, Bowden RA. Brain abscess following marrow transplantation: experience at the Fred Hutchinson Cancer Research Center, 1984–1992. Clin Infect Dis. 1994; 19:402–408.10.1093/clinids/19.3.402 [PubMed: 7811856]
8. Borha A, Parienti JJ, Emery E, Coskun O, Khouri S, Derlon JM. Candida albicans cerebral granuloma in an immunocompetent patient. A case report. Neurochirurgie. 2009; 55:57–62.10.1016/j.neuchi.2008.06.001 [PubMed: 18692208]
9. Parker JC Jr, Cleary TJ, Monji T, Kogure K, Castro A. Modifying cerebral candidiasis by altering the infectious entry route. Arch Pathol Lab Med. 1980; 104:537–540. [PubMed: 6998409]
10. Jong AY, Stins MF, Huang SH, Chen SH, Kim KS. Traversal of Candida albicans across human blood-brain barrier in vitro. Infect Immun. 2001; 69:4536–4544.10.1128/IAI.69.7.4536-4544.2001 [PubMed: 11401997]
11. Liu Y, Mittal R, Solis NV, Prasadarao NV, Filler SG. Mechanisms of Candida albicans trafficking to the brain. PLoS Pathog. 2011; 7:e1002305.10.1371/journal.ppat.1002305 [PubMed: 21998592]
12. Lossinsky AS, Jong A, Fiala M, Mukhtar M, Buttle KF, Ingram M. The histopathology of Candida albicans invasion in neonatal rat tissues and in the human blood-brain barrier in culture revealed by light, scanning, transmission and immunoelectron microscopy. Histol Histopathol. 2006; 21:1029–1041. [PubMed: 16835826]
13. Lossinsky AS, Shivers RR. Structural pathways for macromolecular and cellular transport across the blood-brain barrier during inflammatory conditions. Histol Histopathol. 2004; 19:535–564. [PubMed: 15024715]
14. Bierry G, Jehl F, Neuville A, Lefevre S, Robert P, Kremer S, Dietemann JL. MRI of macrophages in infectious knee synovitis. AJR Am J Roentgenol. 2010; 194:W521–526.10.2214/AJR.09.3768 [PubMed: 20489072]
15. Dardzinski BJ, Schmithorst VJ, Holland SK, Boivin GP, Imagawa T, Watanabe S, Lewis JM, Hirsch R. MR imaging of murine arthritis using ultrasmall superparamagnetic iron oxide particles. Magn Reson Imaging. 2001; 19:1209–1216.10.1016/S0730-725X(01)00448-9 [PubMed: 11755731]
16. Lefevre S, Ruimy D, Jehl F, Neuville A, Robert P, Sordet C, Ehlinger M, Dietemann JL, Bierry G. Septic arthritis: monitoring with USPIO-enhanced macrophage MR imaging. Radiology. 2011; 258:722–728.10.1148/radiol.10101272 [PubMed: 21339348]
17. Andronesi OC, Mintzopoulos D, Righi V, Psychogios N, Kesarwani M, He J, Yasuhara S, Dai G, Rahme LG, Tzika AA. Combined off-resonance imaging and T2 relaxation in the rotating frame for positive contrast MR imaging of infection in a murine burn model. J Magn Reson Imaging. 2010; 32:1172–1183.10.1002/jmri.22349 [PubMed: 21031524]
18. Bierry G, Jehl F, Boehm N, Robert P, Dietemann JL, Kremer S. Macrophage imaging by USPIO-enhanced MR for the differentiation of infectious osteomyelitis and aseptic vertebral inflammation. Eur Radiol. 2009; 19:1604–1611.10.1007/s00330-009-1319-4 [PubMed: 19198846]
19. Bierry G, Jehl F, Boehm N, Robert P, Prévost G, Dietemann J-L, Desal H, Kremer S. Macrophage Activity in Infected Areas of an Experimental Vertebral Osteomyelitis Model: USPIO-enhanced MR Imaging—Feasibility Study1. Radiology. 2008; 248:114–123.10.1148/radiol.2481071260 [PubMed: 18458246]
20. Fukuda Y, Ando K, Ishikura R, Kotoura N, Tsuda N, Kato N, Yoshiya S, Nakao N. Superparamagnetic iron oxide (SPIO) MRI contrast agent for bone marrow imaging: differentiating bone metastasis and osteomyelitis. Magnetic Resonance in Medical Sciences. 2006; 5:191–196.10.2463/mrms.5.191 [PubMed: 17332709]
21. Kruskal JB. Can USPIO-enhanced Spinal MR Imaging Help Distinguish Acute Infectious Osteomyelitis from Chronic Infectious and Inflammatory Processes? Radiology. 2008; 248:1–3.10.1148/radiol.2481080495 [PubMed: 18566162]
22. Wei L, Zhou G, Li Z, He L, Gao M, Tan J, Lei H. Detection of toxoplasmic lesions in mouse brain by USPIO-enhanced magnetic resonance imaging. Magn Reson Imaging. 2007; 25:1442–1448.10.1016/j.mri.2007.04.016 [PubMed: 17614231]

23. Gellissen J, Axmann C, Prescher A, Bohndorf K, Lodemann KP. Extra- and intracellular accumulation of ultrasmall superparamagnetic iron oxides (USPIO) in experimentally induced abscesses of the peripheral soft tissues and their effects on magnetic resonance imaging. Magn Reson Imaging. 1999; 17:557–567.10.1016/S0730-725X(98)00206-9 [PubMed: 10231182]
24. Kaim AH, Wischer T, O'Reilly T, Jundt G, Frohlich J, von Schulthess GK, Allegrini PR. MR imaging with ultrasmall superparamagnetic iron oxide particles in experimental soft-tissue infections in rats. Radiology. 2002; 225:808–814.10.1148/radiol.2253011485 [PubMed: 12461265]
25. Kim KS. Pathogenesis of bacterial meningitis: from bacteraemia to neuronal injury. Nat Rev Neurosci. 2003; 4:376–385.10.1038/nrn1103 [PubMed: 12728265]
26. Lutz AM, Weishaupt D, Persohn E, Goepfert K, Froehlich J, Sasse B, Gottschalk J, Marincek B, Kaim AH. Imaging of macrophages in soft-tissue infection in rats: relationship between ultrasmall superparamagnetic iron oxide dose and MR signal characteristics. Radiology. 2005; 234:765–775.10.1148/radiol.2343031172 [PubMed: 15665219]
27. Hauger O, Grenier N, Deminere C, Lasseur C, Delmas Y, Merville P, Combe C. USPIO-enhanced MR imaging of macrophage infiltration in native and transplanted kidneys: initial results in humans. Eur Radiol. 2007; 17:2898–2907.10.1007/s00330-007-0660-8 [PubMed: 17929025]
28. Yang D, Ye Q, Williams M, Sun Y, Hu TC, Williams DS, Moura JM, Ho C. USPIO-enhanced dynamic MRI: evaluation of normal and transplanted rat kidneys. Magn Reson Med. 2001; 46:1152–1163.10.1002/mrm.1312 [PubMed: 11746582]
29. Ye Q, Yang D, Williams M, Williams DS, Pluempitiwiriyawej C, Moura JM, Ho C. In vivo detection of acute rat renal allograft rejection by MRI with USPIO particles. Kidney Int. 2002; 61:1124–1135.10.1046/j.1523-1755.2002.00195.x [PubMed: 11849467]
30. Zhang Y, Dodd SJ, Hendrich KS, Williams M, Ho C. Magnetic resonance imaging detection of rat renal transplant rejection by monitoring macrophage infiltration. Kidney Int. 2000; 58:1300–1310.10.1046/j.1523-1755.2000.00286.x [PubMed: 10972694]
31. Pedersen M, Laustsen C, Perot V, Basseau F, Moonen C, Grenier N. Renal hemodynamics and oxygenation in transient renal artery occluded rats evaluated with iron-oxide particles and oxygenation-sensitive imaging. Z Med Phys. 2010; 20:134–142.10.1016/j.zemedi.2010.02.002 [PubMed: 20540904]
32. Floris S, Blezer EL, Schreibelt G, Dopp E, van der Pol SM, Schadee-Eestermans IL, Nicolay K, Dijkstra CD, de Vries HE. Blood-brain barrier permeability and monocyte infiltration in experimental allergic encephalomyelitis: a quantitative MRI study. Brain. 2004; 127(Pt 3):616–627.10.1093/brain/awh068 [PubMed: 14691063]
33. Schoepf U, Marecos EM, Melder RJ, Jain RK, Weissleder R. Intracellular magnetic labeling of lymphocytes for in vivo trafficking studies. Biotechniques. 1998; 24:642–646. 648–651. [PubMed: 9564539]
34. McGavern DB, Kang SS. Illuminating viral infections in the nervous system. Nat Rev Immunol. 2011; 11:318–329.10.1038/nri2971 [PubMed: 21508982]
35. Yang G, Pan F, Parkhurst CN, Grutzendler J, Gan WB. Thinned-skull cranial window technique for long-term imaging of the cortex in live mice. Nat Protoc. 2010; 5:201–208.10.1038/nprot.2009.222 [PubMed: 20134419]
36. Igyarto BZ, Haley K, Ortner D, Bobr A, Gerami-Nejad M, Edelson BT, Zurawski SM, Malissen B, Zurawski G, Berman J, Kaplan DH. Skin-resident murine dendritic cell subsets promote distinct and opposing antigen-specific T helper cell responses. Immunity. 2011; 35:260–272.10.1016/j.immuni.2011.06.005, [PubMed: 21782478]
37. Navarathna DH, Hornby JM, Hoerrmann N, Parkhurst AM, Duhamel GE, Nickerson KW. Enhanced pathogenicity of Candida albicans pre-treated with subinhibitory concentrations of fluconazole in a mouse model of disseminated candidiasis. J Antimicrobial Chemother. 2005; 56:1156–1159.10.1093/jac/dki383
38. Raab SS, Cheville JC, Bottles K, Cohen MB. Utility of Gomori methenamine silver stains in bronchoalveolar lavage specimens. Mod Pathol. 1994; 7:599–604. [PubMed: 7524071]

39. Lauterbach H, Zuniga EI, Truong P, Oldstone MB, McGavern DB. Adoptive immunotherapy induces CNS dendritic cell recruitment and antigen presentation during clearance of a persistent viral infection. J Exp Med. 2006; 203:1963–1975.10.1084/jem.20060039 [PubMed: 16847068]
40. Kang SS, Herz J, Kim JV, Nayak D, Stewart-Hutchinson P, Dustin ML, McGavern DB. Migration of cytotoxic lymphocytes in cell cycle permits local MHC I-dependent control of division at sites of viral infection. J Exp Med. 2011; 208:747–759.10.1084/jem.20101295 [PubMed: 21464219]
41. Kim JV, Kang SS, Dustin ML, McGavern DB. Myelomonocytic cell recruitment causes fatal CNS vascular injury during acute viral meningitis. Nature. 2009; 457:191–195.10.1038/nature07591 [PubMed: 19011611]
42. Rubin LL, Staddon JM. The cell biology of the blood-brain barrier. Annu Rev Neurosci. 1999; 22:11–28.10.1146/annurev.neuro.22.1.11 [PubMed: 10202530]
43. Chang YC, Stins MF, McCaffery MJ, Miller GF, Pare DR, Dam T, Paul-Satyaseela M, Kim KS, Kwon-Chung KJ. Cryptococcal yeast cells invade the central nervous system via transcellular penetration of the blood-brain barrier. Infect Immun. 2004; 72:4985–4995.10.1128/IAI.72.9.4985-4995.2004 [PubMed: 15321990]
44. Nakayama H, Shibuya K, Kimura M, Ueda M, Iwabuchi S. Histopathological study of candidal infection in the central nervous system. Nippon Ishinkin Gakkai Zasshi. 2010; 51:31–45.10.3314/jjmm.51.31
45. Haorah J, Ramirez SH, Schall K, Smith D, Pandya R, Persidsky Y. Oxidative stress activates protein tyrosine kinase and matrix metalloproteinases leading to blood-brain barrier dysfunction. J Neurochem. 2007; 101:566–576.10.1111/j.1471-4159.2006.04393.x [PubMed: 17250680]
46. Kahles T, Luedike P, Endres M, Galla HJ, Steinmetz H, Busse R, Neumann-Haefelin T, Brandes RP. NADPH oxidase plays a central role in blood-brain barrier damage in experimental stroke. Stroke. 2007; 38(11):3000–3006.10.1161/STROKEAHA.107.489765 [PubMed: 17916764]
47. Lionakis MS, Lim JK, Lee CC, Murphy PM. Organ-specific innate immune responses in a mouse model of invasive candidiasis. J Innate Immun. 2011; 3(2):180–199.10.1159/000321157 [PubMed: 21063074]
48. Romani L. Immunity to Candida albicans: Th1, Th2 cells and beyond. Curr Opin Microbiol. 1999; 2(4):363–367.10.1016/S1369-5274(99)80064-2 [PubMed: 10458979]
49. Ghosh S, Navarathna DH, Roberts DD, Cooper JT, Atkin AL, Petro TM, Nickerson KW. Arginine-induced germ tube formation in Candida albicans is essential for escape from murine macrophage line RAW 264.7. Infect Immun. 2009; 77(4):1596–1605.10.1128/IAI.01452-08 [PubMed: 19188358]
50. Desestret V, Brisset JC, Moucharrafie S, Devillard E, Nataf S, Honnorat J, Nighoghossian N, Berthezene Y, Wiart M. Early-stage investigations of ultrasmall superparamagnetic iron oxide-induced signal change after permanent middle cerebral artery occlusion in mice. Stroke. 2009; 40(5):1834–1841.10.1161/STROKEAHA.108.531269 [PubMed: 19286601]
51. Lawaczeck R, Bauer H, Frenzel T, Hasegawa M, Ito Y, Kito K, Miwa N, Tsutsui H, Vogler H, Weinmann HJ. Magnetic iron oxide particles coated with carboxydextran for parenteral administration and liver contrasting. Pre-clinical profile of SH U555A. Acta Radiol. 1997; 38(4 Pt 1):584–597. [PubMed: 9240682]
52. Zhang Z, van den Bos EJ, Wielopolski PA, de Jong-Popijus M, Bernsen MR, Duncker DJ, Krestin GP. In vitro imaging of single living human umbilical vein endothelial cells with a clinical 3.0-T MRI scanner. MAGMA. 2005; 18(4):175–185.10.1007/s10334-005-0108-6 [PubMed: 16096808]
53. Stoll G, Bendszus M, Perez J, Pham M. Magnetic resonance imaging of the peripheral nervous system. J Neurol. 2009; 256(7):1043–1051.10.1007/s00415-009-5064-z [PubMed: 19252774]
54. Stoll G, Bendszus M. Imaging of inflammation in the peripheral and central nervous system by magnetic resonance imaging. Neuroscience. 2009; 158(3):1151–1160.10.1016/j.neuroscience.2008.06.045 [PubMed: 18651996]

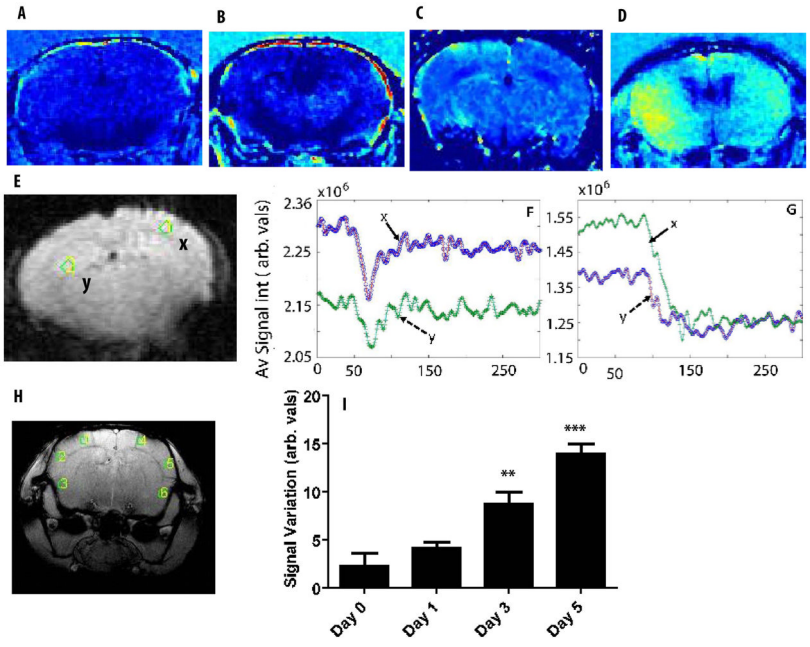

Fig. 1.

Axial images of representative (A) normal and (B,C and D) infected brain after Gd-DTPA infusion. Hyper-intense signals in infected representative brains (n=5) at day 0, 3 and 5 PI show non-localized regions with possible BBB damage in contrast to the normal brain. (E) Two selected ROIs shown in Y and X (10 pixel area) used to assess the dynamic contrast curve after Gd-DTPA infusion for normal mouse (F) and infected mouse brain (G). The normal mouse brain depicts the first pass effects of the contrast agent typical of a brain with intact BBB while the infected regions (G) show effects consistent with BBB breaching. (H) A pilot image showing selected regions of interest (ROI) in cortical areas. (I) The overall average intensity of all selected ROIs plus selected cortical ROIs of penultimate axial slices, showing increase in signal intensity in a quantitative longitudinal study corresponding to Gd-DTPA leakage due to BBB damage in infected mouse in comparison with the normal is summarized. The abbreviated units of 1F, 1G and I is arbitrary values of average signal intensities.

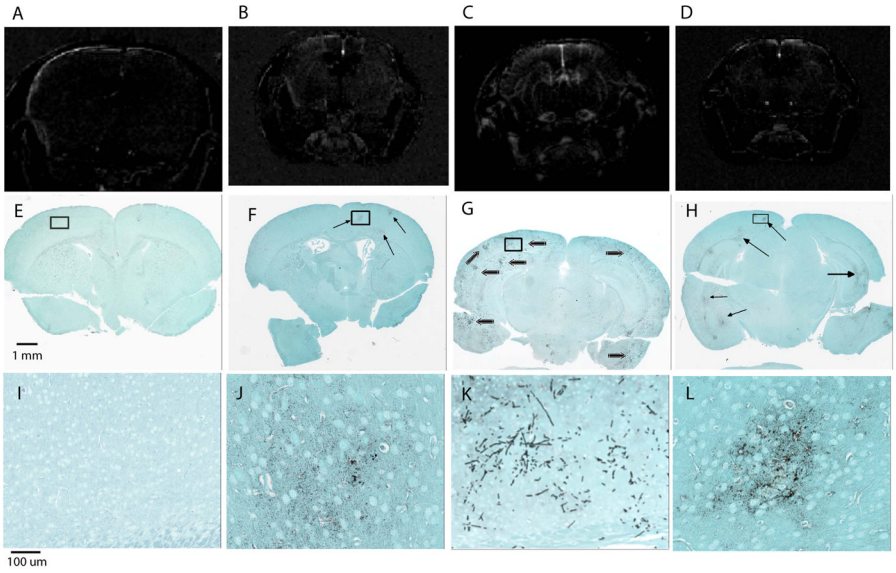

Fig. 2.

Representative axial images of mouse brains after *i.v.* administration of Gd-DTPA in (A) control (B) day 1, (C) day 3 and (D) day 5 PI infected mice and their corresponding, fungal specific, GMS stained sections of the uninfected (E) and infected brains (F–H) with high magnification of selected areas (I–L). No visible changes are observed in the non-infected mouse brain (A) where Gd does not penetrate the BBB. Hyper-intense regions in *C. albicans* infected mice post-Gd infusion show visible differences in all tested time points, consistent with vascular BBB breaching. Furthermore, post Gd signal variation images for *C. albicans* infected mouse brains at three different time points (B–D, n=5) show varying degrees of Gd leakage (BBB breaching) with severity of infection indicated by hyper-intensity of the MRI images correlating well with the observed histology (E–L).

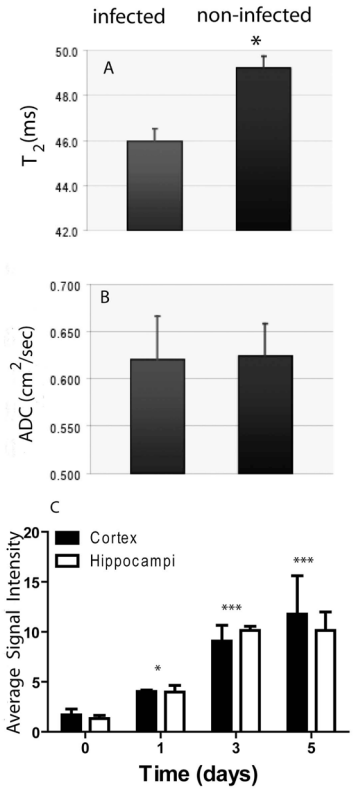

Fig. 3.

(A) Average spin-spin relaxation times (T_2) and (B) apparent diffusion coefficients (ADC) for, multiple cortical ROIs (10 ROIs per region with pixel resolution of 0.0075 cm and 10 pixel area of 5.625×10^{-4} cm^2) over 6 contiguous axial slices, of normal and infected brains. Structural changes in the micro-environment in the cortical areas due to the infiltration of *Candida* correlate with altered cellular integrity in the infected brains, thus leading to reduction in T_2. Perhaps due to the large vacuole present in *Candida* cells, ADC values were not significantly altered by infection. (C) Longitudinal changes in signal intensities of axial images of frontal and dorsal regions of infected brains after Gd-DTPA infusion. Increasing hyper-intense signal in infected brain cortex and hippocampus at days 1–5 PI ($p< 0.05$ 0.001 and 0.001, respectively, n = 5) indicates increasing BBB damage.

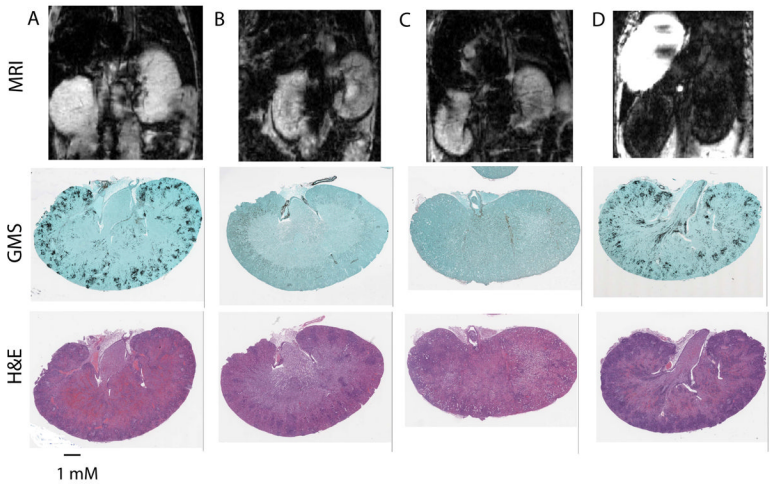

Fig. 4.

C. albicans colonization of the brain was visualized in real-time using intravital TPLSM. A representative maximal projection of a three-dimensional (3D) z-stack shows the distribution of GFP^+ *C. albicans* (green) in the meninges and superficial brain parenchyma three days following infection (low panel). A similar projection captured from an uninfected mouse is shown as a negative control (upper panel). Both the filamentous (white arrows) and yeast (white arrowheads) forms of *C. albicans* were observed by TPLSM. Quantum dots (red) were injected intravenously just before imaging to visualize blood vessels. White scale bars = 50 microns. See associated Movie 1.

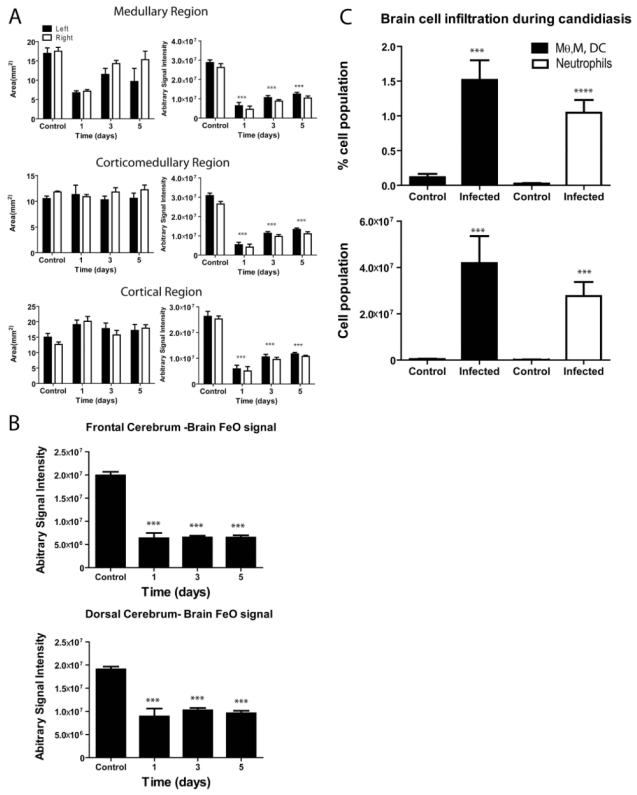

Fig. 5.

Representative sections of transverse MR images of 8 week old BALB/c mice infected with or without *C. albicans* (n=5) and with or without USPIO 24 h post MRI (upper panels) and respective fungal specific GMS and H&E stained sections. (A) Infected mice without USPIO administration do not demonstrate T2* signal loss. Fungal specific GMS shows heavy fugal colonization and H&E section shows inflammatory cell infiltration. (B) Noninfected mice without USPIO administration do not demonstrate T2* signal loss. (C) noninfected mice with USPIO also show no T2* effects. The respective GMS and H&E stained sections in B and C show no colonization and no inflammatory cell infiltration. (D) Infected mouse with USPIO administration clearly demonstrates T2* signal loss. GMS staining shows heavy fugal colonization, and the H&E section shows inflammatory cell infiltration. 1 mm scale bar indicates magnification of the stained sections.

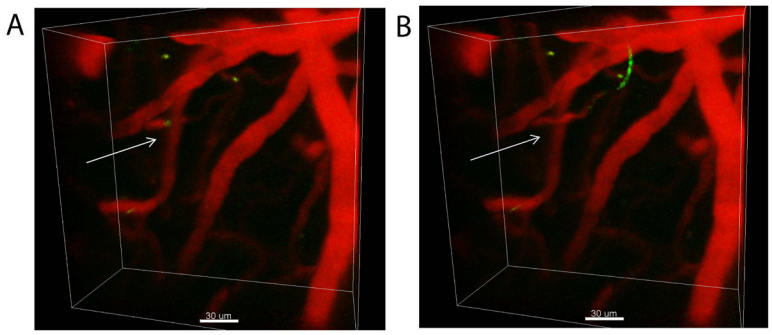

Fig. 6.

T_2^* signal loss in transverse kidney and brain MR images of mice infected with *C. albicans.* Signal was quantified in the indicated regions of kidney and brain 24 hours after injection of USPIO agent and the indicated days post *C. albicans* inoculation. Control 8 week old BALB/c mice were uninfected but received USPIO. (A) Three arbitrarily demarcated medullary, corticomedullary and cortical regions of kidneys were assessed at the indicated times PI for signal intensities (*** $p<0.001$ compared with the control group, consistent with more USPIO-laden phagocytes). (B) T_2^* signal loss was quantified in frontal and dorsal cerebral brain regions at the indicated times post inoculation (*** $p<0.001$). (C) Quantitative analysis of brain infiltrating leukocytes in uninfected and day 3 *C. albicans* infected mice. Bar graphs show the frequency (upper panel) and absolute numbers (low panel) of neutrophils ($CD45^+$ $Thy1.2^-$ $Ly6C^+$ $Gr\text{-}1^{hi}$) and monocytes/macrophages/dendritic cells ($CD45^+$ $Thy1.2^-$ $Ly6C^+$ $Gr\text{-}1^{low}$). Data are presented as the mean±SD. Each group consisted of five mice.